Consolidation of cobalt nanorods: A new route for rare-earth free nanostructured permanent magnets

Semih Ener, Evangelia Anagnostopoulou, Imants Dirba, Lise-Marie Lacroix, Frédéric Ott, Thomas Blon, Jean-Yves Piquemal, Konstantin P Skokov, Oliver Gutfleisch, G. Viau

Consolidation of cobalt nanorods: a new route for rare-earth free nanostructured permanent magnets

Semih Ener [a,†], *Evangelia Anagnostopoulou* [b,†], *Imants Dirba* [a], *Lise-Marie Lacroix* [b], *Frédéric Ott* [c], *Thomas Blon* [b], *Jean-Yves Piquemal* [d], *Konstantin P. Skokov* [a], *Oliver Gutfleisch* [a], *Guillaume Viau* [b,*]

[a] Funktionale Materialien, Institut für Materialwissenschaft, TU Darmstadt, Alarich-Weiss-Str. 16, D-64287 Darmstadt, Germany

[b] Université de Toulouse, Laboratoire de Physique et Chimie des Nano-Objets, UMR 5215 INSA, CNRS, UPS, 135 avenue de Rangueil, F-31077 Toulouse cedex 4, France

[c] Laboratoire Léon Brillouin CEA/CNRS, Université Paris-Saclay, CEA Saclay, 91191 Gif sur Yvette, France

[d] Université Paris Diderot, Sorbonne Paris Cité, ITODYS, CNRS UMR 7086, 15 rue J.-A. de Baïf, 75205 Paris Cedex 13, France

[†] both authors contributed equally to this work

* Corresponding author
e-mail adress : gviau@insa-toulouse.fr (G. Viau)

Abstract

Rare-earth free permanent magnets were produced by consolidation of cobalt nanorods synthesized by the polyol process exhibiting a mean diameter in the range 10 to 30 nm. Compactions of magnetically prealigned rod assemblies at various pressures and temperatures were carried out to make dense materials. Bulk magnets exhibiting a very good mechanical strength and an energy product as high as 65 $kJ.m^{-3}$ were obtained. The best results were obtained when the compaction conditions were soft enough to preserve the morphology and alignment of the rods in the final material, as revealed by X-ray diffraction and neutron scattering. For the first time the bottom-up approach is convincingly reported to produce bulk magnets without the addition of any matrix, the obtained nanostructured materials exhibit coercivity much higher than the AlNiCo magnets and can fill the performance "gap" between hexaferrites and rare-earth based magnets.

Keywords

Cobalt nanorods; permanent magnets; bottom-up; energy product; consolidation process

1. Introduction

Permanent magnets (PMs) are microstructured materials designed to generate perpetual magnetic fields outside their volume, known as stray fields. These materials are essential for power sources, which spread from the biggest scale as in wind power generators to the submillimeter scale as in integrated sensors and actuators [1,2]. The strength of a PM is characterized by the energy product - or $(BH)_{max}$ - corresponding to the maximum energy stored [3,4]. To reach a high energy product a magnetic material must combine a high remanent magnetization (M_r) with a high coercivity (H_C). The permanent magnet market is dominated mainly by two types of materials: (i) the high performance rare-earth (RE) transition metal (TM) alloys, $(BH)_{max} > 250$ kJ.m^{-3}, and (ii) the inexpensive but low performance Ba- and Sr-hexaferrites materials, $(BH)_{max} < 40$ kJ.m^{-3}, while the AlNiCo magnets that consist in ferromagnetic Fe-Co needles within a Ni-Al-rich matrix formed via spinodal decomposition are still used for high temperature applications [1].

After the RE supply crisis in 2011, new materials capable of filling the "gap" between hexaferrites and RETM alloys have been intensively sought [4]. One strategy consists in exploring high magneto-crystalline anisotropy alloys through combinatorial methods [5,6]. Among the different candidates, Mn- and Fe- based alloys [7,8,9] are meeting the abundance criterion, while Co-based alloys [10,11,12] benefit from the high intrinsic anisotropy of cobalt. The challenge consists now in preparing bulk magnets, any deviation from the optimal composition or crystallographic phase drastically impact the magnetic properties [13].

The alternative route consists in assembling magnetic nanoparticles (NPs) into dense nanostructured PM following a bottom-up approach [14]. Providing a single-domain configuration and a sufficient coercivity of the building blocks, performant PM should be obtained [13]. In that aim, the magnetic anisotropy of nanoparticles can be enhanced by an antiferromagnetic shell [15] or by playing with the particle shape [16]. Magnetic nanorods (NRs) and nanowires (NWs), when properly grown, can indeed combine shape and magnetocrystalline anisotropies. The possibility of coupling these two anisotropy sources stimulated researches on high density magnetic data storage [17] and permanent magnet applications [18]. The coercivity of cobalt NRs is strongly dependent on their size, shape and crystalline structure [19,20]. Several groups worldwide have recently measured relatively high coercivity on single-crystalline *hcp* cobalt rods and wires prepared following polyol process and organometallic approaches [21,22].

With the aim of preparing integrated magnets on Micro-Electro Mechanical Systems (MEMS), magnetic particles immersed in a polymer matrix have been patterned using inkjet [23], imprinting [24] or photolithography techniques [25]. Alternatively, electroplating through masks [26,27] have been recently investigated. However, all these approaches suffer from the dilution of the magnetic building blocks to ensure a proper mechanical strength. The final nanocomposites exhibit accordingly a low magnetic fraction, which drastically reduce the PM performances. One natural idea consists therefore in benefiting from the consolidation techniques which have been intensively developed for permanent magnets. Spark plasma sintering and mechanical densification techniques have proven their efficiency to compact chemically grown NPs into exchange-spring magnets. However, the severe experimental conditions usually yield a partial sintering of the building blocks [28,29,30].

Starting from *hcp* Co rods with as aspect ratio, the challenge consists here in obtaining dense and highly textured materials with high magnetic performances using consolidation methods soft enough to : (i) preserve the rod morphology, preventing their coalescence and (ii) avoid the phase transformation of Co *hcp* to Co *fcc* which occurs at 450°C [31]. Thus, consolidation conditions should be limited to fairly mild ones. Ouar *et al.* introduced a spark plasma sintering method for the consolidation of $Co_{80}Ni_{20}$ nanowires which is up to now the only consolidation study on nanowire arrays [32,33]. In their work, a remanence-to-saturation values of only 0.53 was measured when the applied field was along the easy axis for powder and consolidated samples, revealing a non-optimized alignment.

In this work, we propose alternative consolidation and densification routes for cobalt nano-rods to yield performant permanent magnets. Cobalt NRs with different diameters were produced and compacted under different conditions. The magnetic properties and the performance of the consolidated magnets are discussed in relationship with their microstructure analyzed by neutron scattering and X-ray diffraction.

2. Experimental

2.1. Nanorods preparation

Cobalt(II) acetate was purchased from Alfa Aesar, sodium hydroxide, lauric acid, 1,2-butanediol and oleylamine from Acros, hydrated ruthenium chloride from Sigma-Aldrich (ref. Sigma Aldrich 84050). All the raw chemicals were used without additional purification. Cobalt nanorods were prepared by the polyol process, up-scaling a procedure previously described

[18]. Cobalt(II) laurate, $Co(C_{12}H_{23}O_2)_2$, xH_2O, was prepared by mixing equimolar aqueous solutions of cobalt acetate and sodium laurate. The pink precipitate was washed with de-ionized water and dried overnight at 50°C in order to remove the water excess. Thermogravimetric analysis of the cobalt laurate precursor was performed to confirm that the water/Co molar ratio, x, was lower than 2 before using. The reduction of cobalt laurate in a basic solution of 1,2 butanediol was performed in a 3L jacketed reactor heated by a hot oil flow. 39.5 g of cobalt laurate (8×10^{-2} mol.L^{-1}) were dispersed in 1L of a solution of sodium hydroxide (3 g, 7.5×10^{-2} mol.L^{-1}) in 1,2 butanediol. Ruthenium chloride (0.5g, [Ru]/[Co] = 2.5%) was added to control the nucleation step. The suspension was heated to 175 °C for 20 min under mechanical stirring. The stirring speed was varied in the range 40-160 rpm. The solution turned black at 170°C indicating the cobalt reduction. The cobalt suspension was cooled down to room temperature, washed twice with absolute ethanol and twice with chloroform. The yield of the cobalt reduction was very close to 100 %.

The cobalt rods were separated from the butanediol by centrifugation, washed with absolute ethanol till the supernatant was colourless, and washed with chloroform. Rod assemblies were prepared by controlled evaporation at room temperature of suspensions in chloroform in an electromagnet under a magnetic field of 1T.

2.2. Nanorods consolidations

Consolidations of the nanorods were done by using two different compaction techniques: cold compaction (CC) and hot compaction (HC). Prior to the consolidation "green-compacts" were prepared by doing a pre-alignment of the rod assemblies. A 1.7 T electromagnet was used for the preparation of the green-compacts in the consolidation dies. The cold compaction was carried out on the same uniaxial hydraulic press used for the green-compacts preparation. For cold compaction, the highest pressure was 1 GPa. The hot compaction studies were done on a hot press equipped with twelve halogen lamps for heating the sample, the upper pressure was in that case limited to 450 MPa. During the hot compaction, the temperature of the die is kept at 180 ºC and the nanorods were compacted at various pressures for 2 minutes. The control of the temperature during the consolidation has essential importance as previous studies showed that coalescence of nanorods can start at 220 °C [31].

2.3. Characterizations

Transmission electron microscopy (TEM) characterizations on the cobalt nanorods were performed using a JEOL 1400 microscope operating at 120 kV. Scanning electron microscopy

(SEM) characterizations on rod assemblies before compaction were performed using a JEOL JSM 6700F microscope. Powder X-ray diffraction measurements were carried out using a PANalytical Empyrean diffractometer equipped with an X'celerator detector using Co Kα radiation. The X-ray diffraction measurements on consolidated magnets were performed on a θ-2θ 4-circles stage using a Ge(220) monochromator to select the CoKα1 radiation ($\lambda_{K\alpha1}$ = 1.78891 Å). Compacted bulk magnets were characterized by Small Angle Neutron Scattering (SANS) at the Laboratoire Léon Brillouin on the spectrometer PA20.[34] The neutron wavelength was set at 6Å. The magnetic properties of the rod assemblies before consolidation were characterized using a Quantum Design Physical Property Measurement System (PPMS) with the Vibrating Sample Magnetometer (VSM) configuration. The magnetic properties of the compacted magnets were measured with a Metis pulse magnetometer. The demagnetization corrections were done by using the shape and dimensions of the consolidated products. The hysteresis measurements were done in the external field interval of -3.6 to +3.6 T. Magnetic measurements of the bulk magnets were done with the applied field parallel to the direction of the applied external magnetic during the preparation of the "green bodies". The induction per volume *B* was calculated as the ratio of the induction of the sample over the volume of the sample. The magnetic volume fraction, V_M, was calculated as the ratio of the saturation magnetization per volume of the sample divided by the bulk saturation magnetization (1.79 T).

3. Results and Discussion

3.1. Parallel assemblies of cobalt nanorods with controlled mean diameter

The challenge for consolidation experiments and the preparation of macroscale magnets consisted in preparing several grams of cobalt rods in a single batch using a scale-up process. The cobalt particles prepared by heating 39.5 g of cobalt laurate in 1L of 1,2 butanediol exhibited anisotropic shapes as showed in the TEM micrographs (Figure 1). The morphology was found to strongly depend on the stirring applied during the cobalt growth. For a stirring speed of 160 rpm, rough NRs exhibiting a mean diameter of *ca.* 30 nm were obtained (Fig. 1a). At 60 rpm, the mean diameter decreased to *ca.* 10 nm. The NRs surface was smooth, leading to a regular diameter all along the rod length (Fig. 1b). X-ray diffraction showed that the rods crystallize with the *hcp* structure. The (0002) XRD line was always found much narrow than the $(10\bar{1}0)$ line, this broadening contrast is in agreement with the *c* axis laying parallel to the

long axis as previously reported on small scale synthesis [35]. The crystallite size $L_{(10\bar{1}0)}$ measured from the $(10\bar{1}0)$ reflexion broadening using the Scherrer equation was found very close to the particle mean diameter measured by TEM (Fig. S1).

After synthesis, the rods were washed to remove organic the excess of leftovers and surfactant prior drying. Preliminary experiments showed that magnetically random powders could not be further aligned during the compaction process. Despite the application of a magnetic field of 1.7 T during the consolidation, the remanence to saturation ratio, M_r/M_s, of materials prepared from such random powders was limited to 61 %. Such a low value is detrimental for the magnet performance and cannot lead to high $(BH)_{max}$ [3]. In order to circumvent this problem, the rods were first dried under an external field of 1 T to produce pellets that exhibited a very good cohesion before compaction (Fig. 2a). These pellets consist in dense and highly parallel organizations of nanorods as evidenced by the SEM micrographs (Fig. 2b-c). This anisotropy was confirmed by magnetic measurements. Square hysteresis loops with remanent to saturation ratio M_r/M_s close to 1 were measured in the parallel configuration while the loops were almost closed in the perpendicular configuration (see supplementary materials Fig. S2). The highest M_r/M_s value (0.97) was obtained for the rod exhibiting mean diameter of d_m = 20.4 nm and mean aspect ratio of AR = 4.5 (Fig. S2b). A lower value (M_r/M_s = 0.86) was obtained with the long and thin rods (d_m = 10.9 nm, AR = 18). This difference can be attributed to the difficulty encountered when aligning high aspect ratio rods, leading to a poorer alignment quality. For the thicker rods (d_m = 28.3 nm, AR = 6.7), a M_r/M_s value of 0.89 was measured despite a very nice alignment, observed on the SEM images. In that case we attribute this lower value to a lower nucleation field due to the larger rod diameter and the presence of morphological and structural defects [19].

The coercivity of the *M(H)* loop in parallel configuration was found to increase when the Co NRs mean diameter decreased (Fig. S2). The measured coercivity varied between 288 kA.m^{-1} ($\mu_0 H_C$ = 0.36 T) for d_m = 28.3 nm, to 374 kA.m^{-1} ($\mu_0 H_C$ = 0.47 T) for d_m = 20.4 nm and to 486 kA.m^{-1} ($\mu_0 H_C$ = 0.61 T) for d_m = 10.9 nm. These variations are in good agreement with previously reported micromagnetic modelling. The magnetization reversal in nanorods proceeds indeed non-homogeneously through (i) nucleation of a reversed domain at the tips and (ii) propagation by domain wall motion. Therefore, by decreasing the mean diameter, the

volume of nucleation becomes smaller, leading to a larger nucleation field and a higher coercivity [19,36].

3.2. Magnetic and structural properties of the consolidated materials

The consolidations of the rod assemblies were performed without adding any matrix. The dilution of the active magnetic volume would indeed result in a lower magnetization, as observed in the bonded magnets. Bulk magnets exhibiting different outer shape, as shown in Figure 4, could be prepared from Co nanorods using different compaction methods. Interestingly, the compacted materials maintain their integrity even after shaping/cutting, despite the absence of solid matrix. Magnets I-IV prepared by consolidation of pre-aligned rods with the two extreme mean diameters, 10.9 nm and 28.3 nm, were analyzed in detail. The consolidation conditions are given in Table 1.

The XRD patterns of the consolidated materials were recorded in θ-θ configuration with the alignment direction parallel to the diffraction plane (see supplementary materials Fig. S3). The patterns exhibit the (*hkil*) reflections of the *hcp* Co. No trace of *fcc* Co was detected due to the precisely controlled consolidation temperature during the hot compaction (180°C) which is clearly lower than the *hcp* → *fcc* phase transition. In addition, very broad peaks corresponding to CoO reflections were also detected for the magnets prepared with the thinnest rods revealing a thin oxide shell at the rods surface (Fig. S3). It is noteworthy that the $(10\bar{1}0)$ and $(11\bar{2}0)$ reflections in the XRD patterns are more intense for the consolidated materials than for the powders. In contrast, the (0002) reflection is nearly extinguished in the pattern for consolidated materials (Fig. S3). This is in good agreement with a preferential in-plane orientation of the nanorods long axis (see supplementary materials Fig. S4).

Small angle neutron scattering (SANS) measurements were performed in order to probe the microstructure of the consolidated samples. SANS is the ideal tool for the characterization of bulk materials in comparison to the x-rays due to its deeper penetration depth from the surface. Analysis of the SANS pattern allows an assessment of the rod alignment and a measurement of the mean inter-rod distance. The texture of the rod assemblies is revealed by the anisotropy of the SANS pattern that can be quantified by plotting I_{perp}/I_{para} corresponding to the ratio of the scattering intensity perpendicular and parallel to the rods (Fig. 5). This ratio is 1 for an isotropic system and increases as the system becomes more anisotropic. The comparison of the SANS patterns of magnets II and III illustrates the effect of consolidation conditions on the

microstructure (Fig. 5a,b). The magnet II exhibits an almost isotropic SANS pattern showing the loss of anisotropy after hot compaction under 450 MPa. On the contrary, the magnet III prepared with the same rods compacted at room temperature under 1 GPa exhibits an anisotropic SANS pattern. The two symmetrical correlation peaks perpendicular to the rod long axis shows a parallel arrangement of the rods in this magnet. The cold compaction at 1 GPa is found to be less detrimental for the alignment in comparison with the hot compaction at 450 MPa. The SANS pattern of the magnet IV also exhibits an anisotropic feature with two correlation peaks, showing that, for given consolidation conditions, the alignment is more robust with thicker rods.

The mean inter-rod distance D_m was calculated from the structure factor $S(q)$ of the scattering intensity perpendicular to the rod long axis. D_m is related to the q position of the correlation peak of $S(q)$ according to $q_{\perp max} = 2\pi/D_m$. D_m was found equal to 12.8 nm and 30.0 nm in magnets III and IV (Fig. S5e, see more details in the supplementary materials). These distances are larger than the respective mean diameter showing that rod coalescence did not occur during the consolidation of the magnet. The corresponding mean spacing between the rods is 1.9 nm and 1.7 nm in magnets III and IV, respectively.

The magnetic properties of the magnets I-IV are summarized in Table 1 and the first and second quadrants of the $M(H)$ loops are plotted in Fig. 6. The remanent magnetization $\mu_0 M_r$ varied between 0.39 and 0.82 T. The magnetic volume fractions, calculated as $V_M = M_{(3.6T)}/M(Co_{bulk})$, were found in the range 25-65 % depending on the consolidation experiment and on the rod mean diameter. For a given mean diameter, V_M increased with the pressure applied during the compaction and for given compaction conditions V_M is found much higher for magnets prepared with the thicker rods (Tab. 1). The influence of the rod diameter on the magnetic volume fraction was confirmed by the density values measured by pycnometry. For the same consolidation conditions (HC 450 MPa), the magnet density increased from about 5.2 g.cm^{-3} to 7.1 g.cm^{-3} for rod diameter varying from 10.9 nm to 28.3 nm (Tab. 1). As they were handled in air, the cobalt nanorods were coated by a thin layer of cobalt oxide. The relative amount of cobalt oxide is expected to increase when the rod diameter decreases. Moreover, organic leftover are remaining at their surface and a higher amount is expected in the rod assemblies with the thinner diameter because they exhibit a higher specific surface area. Thus, for a given consolidation conditions one expects to find a higher magnetic volume fraction with the thicker rods.

For a given rod diameter, the quality of the rods alignments in the consolidated magnets was also assessed by the remanence to saturation ratio M_r/M_s. In assemblies of single-domain particles, the squareness of the *M(H)* loop is related to the distribution of the easy-axis orientation with respect to the applied field [16]. Consolidated materials of 10.9 nm rods carried out by hot compaction at 300 MPa and cold compaction at 1 GPa exhibited M_r/M_s ratio very close to the starting assembly, 0.81 and 0.82 in the magnets I and III for 0.86 in the pre-aligned rods (Tab. 1) showing that the texture of the pre-aligned sample was not altered by the consolidation. Under more severe conditions (hot compaction under 450 MPa, magnet II) M_r/M_s felt to 0.69 showing an important deterioration of the rod alignment. In comparison, the relative decrease of M_r/M_s was of less extent, only by 17 %, with the 28.3 nm rods that were also hot compacted under 450 MPa (Tab. 1). This variation of M_r/M_s is in good agreement with the pole figures and SANS measurements that showed a much better rod alignment in magnets III and IV than in II.

The coercivity of the compacted magnets was always found lower than that of the pre-aligned assemblies. For the 10.9 nm rods, H_C decreased by 14 % after HC under 300 MPa and by 31 % after HC under 450 MPa or after CC under 1 GPa (Tab. 1). For the 28.3 nm rods (IV), H_C decreased by 22 % compared to the pre-aligned assembly. An increase in the particle mean size and/or loss of shape anisotropy could decrease the coercivity substantially [36]. Nevertheless, since the rod coalescence was discarded by SANS measurements, the decrease of coercivity observed with densification may be due to increasing dipolar interactions.[37,38]

Finally, the energy products $(BH)_{max.}$ were found between 20 and 65 $kJ.m^{-3}$ (Tab. 1). The comparison of magnets II and III shows that for a given magnetic volume fraction $(BH)_{max}$ increases with the quality of the alignment assessed by the squareness of the *M(H)* loop, the SANS pattern and the XRD pole figures. For a given alignment (M_r/M_s ratio), the $(BH)_{max}$ increases with the magnetic volume fraction as evidenced by the comparison of magnets I and III. Finally, the comparison of magnets III and IV highlights the importance of a high volume fraction to reach high $(BH)_{max}$. Thus, at this point of the study, thicker rods are better suited than thin rods to prepare performant PM.

3.3. Discussion

The permanent magnets obtained by consolidation of cobalt nanorods exhibit a very good mechanical strength even in the absence of matrix additives. This strong cohesion is explained

by a very short inter-rod distance (< 2 nm) as shown by the SANS measurements. The organic leftovers which were not completely removed during the washing process hinder the rod coalescence as evidenced by the contrast of the neutron scattering. These organic molecules remaining at the Co NR surface are mainly the long chain carboxylate (laurate anions) that are present in the cobalt precursor. Previous study including DFT calculations showed that these laurate anions are strongly bounded to the cobalt surface [39]. They play the role of spacers between the rods that maintain the rod morphology and hence a high coercivity.

The energy product reached by the consolidated nanorods is equal or higher than the commercial magnets based on hexaferrites. The comparison with the different grades of anisotropic cast AlNiCo magnets is more relevant since they are also based on the shape anisotropy of iron-cobalt needles in a metallic matrix [40]. The nanorod-based magnets exhibit $(BH)_{max.}$ of same order of magnitude than the AlNiCo magnets. The magnet IV competes with the best commercial grades (AlNiCo9) thanks to its high B_r value. The main advantage of the nanorod-based magnets compared to AlNiCo is their higher coercivity, more than 5 times the coercivity of standard AlNiCo magnets and more than twice the coercivity of the hardest ones [40]. In permanent magnets, a high coercivity value is important to fully benefit from the magnetization in the energy product and also to prevent from irreversible demagnetization [3, 37]. The nanorod-based magnets described here are not coercivity limited which means that there is no limitation on the magnet shape contrary to the AlNiCo. It means also that there is still room to increase the energy product by increasing the remanence.

High energy product could be obtained with higher quality of alignment to improve the *M(H)* loop squareness and higher magnetic volume fraction to improve B_r [18]. In order to determine the key parameters for the improvement of the nanorod-based magnets, a comparison with ideal hexagonal arrays of nanorods is a useful guideline. The magnets can be described as composites with three components, the cobalt core with a thin oxide shell and an organic coating. Previous studies showed that the cobalt oxide (CoO) shell thickness is generally comprised between 1.0 and 1.4 nm [41] and that the resulting volume fraction cannot be neglected [18]. Moreover, organic molecules are present at their surface and their volume fraction is not negligible either [18]. Considering a dense hexagonal array of infinite cobalt wires with the interwire spacing filled by the ligands the theoretical volume fractions of Co, CoO and ligands can be calculated following:

$$V_{Co} = \frac{2\pi(d/2-e)^2}{\sqrt{3}D^2} \quad \text{(Eq. 1)}$$

$$V_{CoO} = \frac{2\pi[(d/2)^2-(d/2-e)^2]}{\sqrt{3}D^2} \quad \text{(Eq. 2)}$$

$$V_L = 1 - V_{CoO} - V_{Co} \quad \text{(Eq. 3)}$$

with d the rod mean diameter inferred from the TEM images, e the CoO shell thickness estimated to 1.2 nm and D the inter-rod distance inferred from the SANS pattern.
Moreover the density of the ideal hexagonal array is given by:

$$\rho = V_{Co} \times \rho_{Co} + V_{CoO} \times \rho_{CoO} + V_L \times \rho_L \quad \text{(Eq. 4)}$$

with Vi and ρi the volume fraction and density of the different components.

Considering rods with a diameter d = 10.9 nm and an inter-rod distance $D = D_m$ = 12.8 nm, the ideal hexagonal array would exhibit a magnetic volume fraction V_{Co} = 40 %, slightly higher than the experimental magnetic volume fraction of magnet III, V_M = 34 % (Tab. 1). Assuming the density of bulk materials, ρ_{Co} = 8.9 g.cm^{-3}, ρ_{CoO} = 6.44 g.cm^{-3} and ρ_L = 0.9 g.cm^{-3}, the theoretical density of the hexagonal arrays is found equal to ρ = 5.5 g.cm^{-3} again slightly higher than the experimental value measured on magnet III ρ = 5.0 g.cm^{-3}. With a 28.3 nm diameter and a 30 nm inter-rod distance, the magnetic volume fraction of the hexagonal array V_{Co} = 67.5 % is very close to the experimental magnetic volume fraction of magnet IV, V_M = 64 % (Tab. 1). The density of the ideal hexagonal array ρ = 7.0 g.cm^{-3} is also very close to the experimental value measured on magnet IV ρ = 7.1 g.cm^{-3}.
Even if the hexagonal arrays are idealistic scheme because the alignment in the real magnets is not perfect and the rods exhibit a limited length, the comparison between the experimental results and ideal arrays allows to conclude on a compact microstructure and on the absence of internal macro- or meso-porosity in the magnets. The presence of large internal voids in the nanostructured magnet can be discarded. The experimental conditions were optimized to consolidate metal nanorods into dense and cohesive materials. The cold compaction at 1 GPa is found better than the hot compaction at 450 MPa since it is mild enough to preserve a good alignment while being strong enough to reach high volume fraction.

The source of improvement may come from the rod optimization. On one hand, rods with large diameter are more interesting to reach high magnetic volume fraction, but on the other hand, the magnets prepared with large rods exhibit a lower coercivity. The next challenge is thus to increase the magnetic volume fraction with thin rods. Much higher volume fraction could be reached if the rod oxidation was avoided. Indeed, assuming an ideal array of non-oxidized rods with mean diameter d_m = 10.9 nm and an inter-rod distance of 12.8 nm, the volume fraction would be 66 % leading to much higher $(BH)_{max}$. Using forming gas atmosphere during the synthesis and consolidation process could be a way to avoid the formation of a cobalt oxide shell. For a cobalt volume fraction of 66 % and a perfect alignment, B_r would reach 1.18 T. In order to have a magnet that would not be coercivity limited $\mu_0 H_C$ value higher than $B_r/2$ must be targeted, i.e. 0.59 T in this case. Coercivity values higher than this critical value have already be obtained by decreasing the particle diameter using organometallic route [22,42] or polyol route [19] or by improving the NR shape as well [43].

4. Conclusion

In this work, a novel production route for a bulk rare-earth free hard magnetic system has been developed. The synthesis of the Co nanorods was successfully scaled up to several gram of cobalt in a single batch and there is no technical limitation of the polyol process to several tens grams at laboratory scale. These rods that combine shape and magnetocrystalline anisotropy exhibit high coercivity thanks to a fine control of their mean diameter and their crystallinity. Consolidation experiments of the nanorods were carried out in absence of any additional polymer matrix. The magnetic volume fraction and density of the consolidated materials are consistent with a compact microstructure without internal porosity. The ligand layer remaining at the nanorods surface both prevents from the rod coalescence and gives a good cohesion/mechanical strength to the consolidated materials.

The resulting bulk consolidated materials, shows energy products as high as 65 $kJ.m^{-3}$, competing with most of anisotropic cast Alnico grades commercially available. Significant improvements are expected by increasing the magnetic volume fraction if the rod oxidation is avoided. Moreover, their high coercivity allows the preparation of bulk magnets without any shape limitation which is the main drawback of the AlNiCo. This work is the first proof-of-concept that the shape anisotropy combined with moderate magnetocrystalline anisotropy can be used to elaborate bulk magnets with interesting performances. This prompts us to extend this idea to other hard magnetic materials.

As far as applications are concerned, the cobalt abundancy may be a problem for using the proposed sample preparation for big scale systems. Nevertheless, the great advantage of the bottom-up approach compared to metallurgical routes is the facility to prepare small size magnets with any desired shape. We think that this route is promising for submillimeter sized magnets suitable for micro-electronic applications.

Supporting Information

Additional data on X-ray diffraction, magnetization curves and small angle neutron scattering (SANS) are available in supporting information.

Acknowledgments

Authors are grateful to the European Community's Seventh Framework Programme for supporting this study with FP7/2007-2013 under Grant agreement number EU NMP3-SL-2012-280670 (Rare Earth Free Permanent Magnets - REFREEPERMAG).

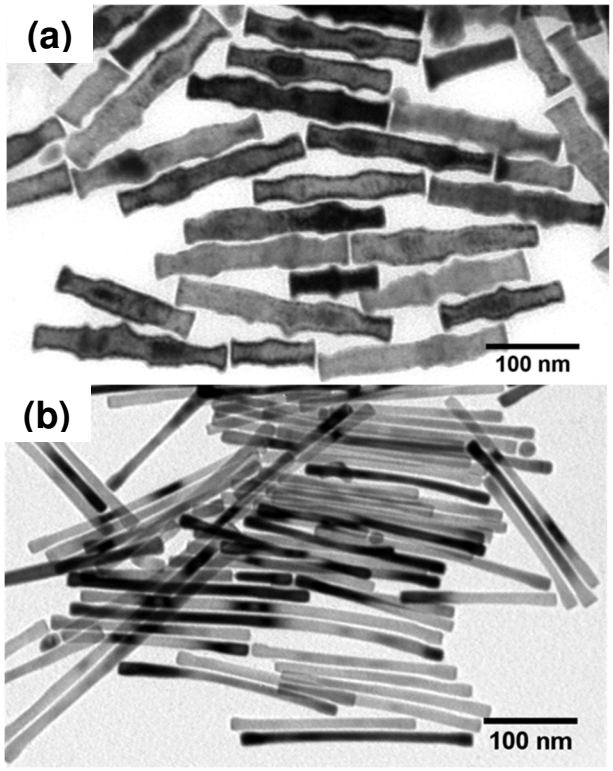

Figure 1. TEM micrographs of cobalt nanorods prepared by the up-scale polyol process (5 g of cobalt per batch) under a stirring speed of (a) 160 rpm and (b) 60 rpm. The mean diameter (d_m) and mean length (L_m) were determined by measuring 100 rods: (a) d_m = 28.3 nm (σ = 4.0 nm), L_m = 190 nm; (b) d_m = 10.9 nm (σ = 1.1 nm), L_m = 200 nm.

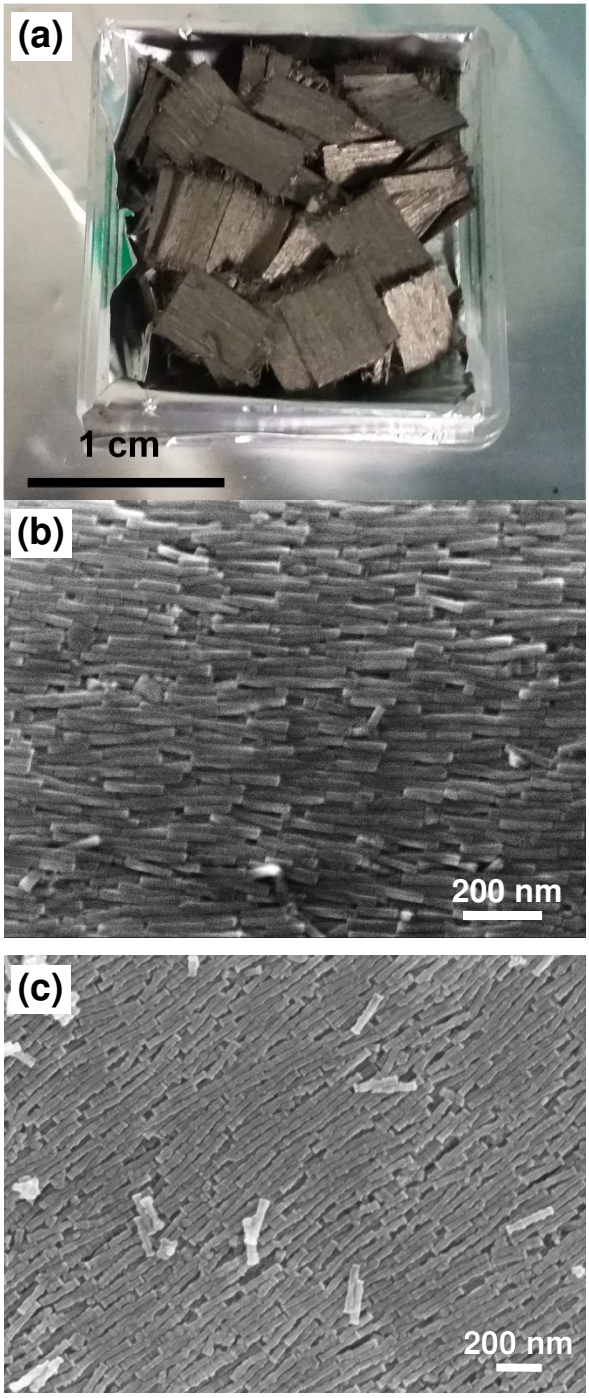

Figure 2. (a) Pellets prepared by drying of Co NRs under a magnetic field of 1 T SEM micrographs of the pellets showing the Co NRs alignments: with mean diameter d_m = 20.4 nm (b) and d_m = 28.3 nm (c).

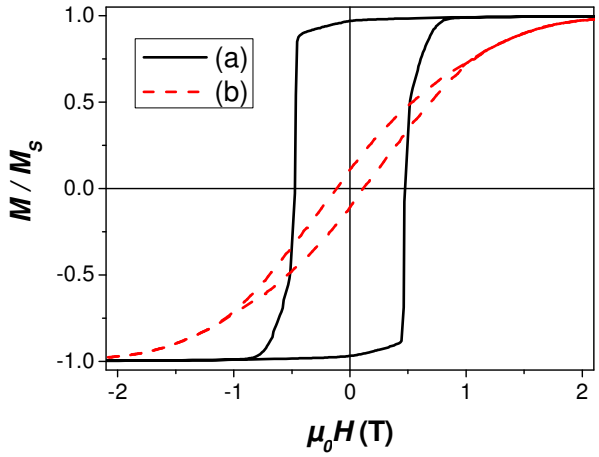

Figure 3. Hysteresis loops of an assembly of Co NRs (d_m = 20.4 nm) measured with the applied field parallel (a) or perpendicular (b) to the rod alignment direction.

Figure 4. Images of consolidated Co nanowires in different shapes. d_m = 10.9 nm compacted at 300 MPa, 180°C (I) ; 450 MPa, 180°C (II); 1GPa, RT (III) ; and d_m = 28.3 nm compacted at 450 MPa, 180°C (IV).

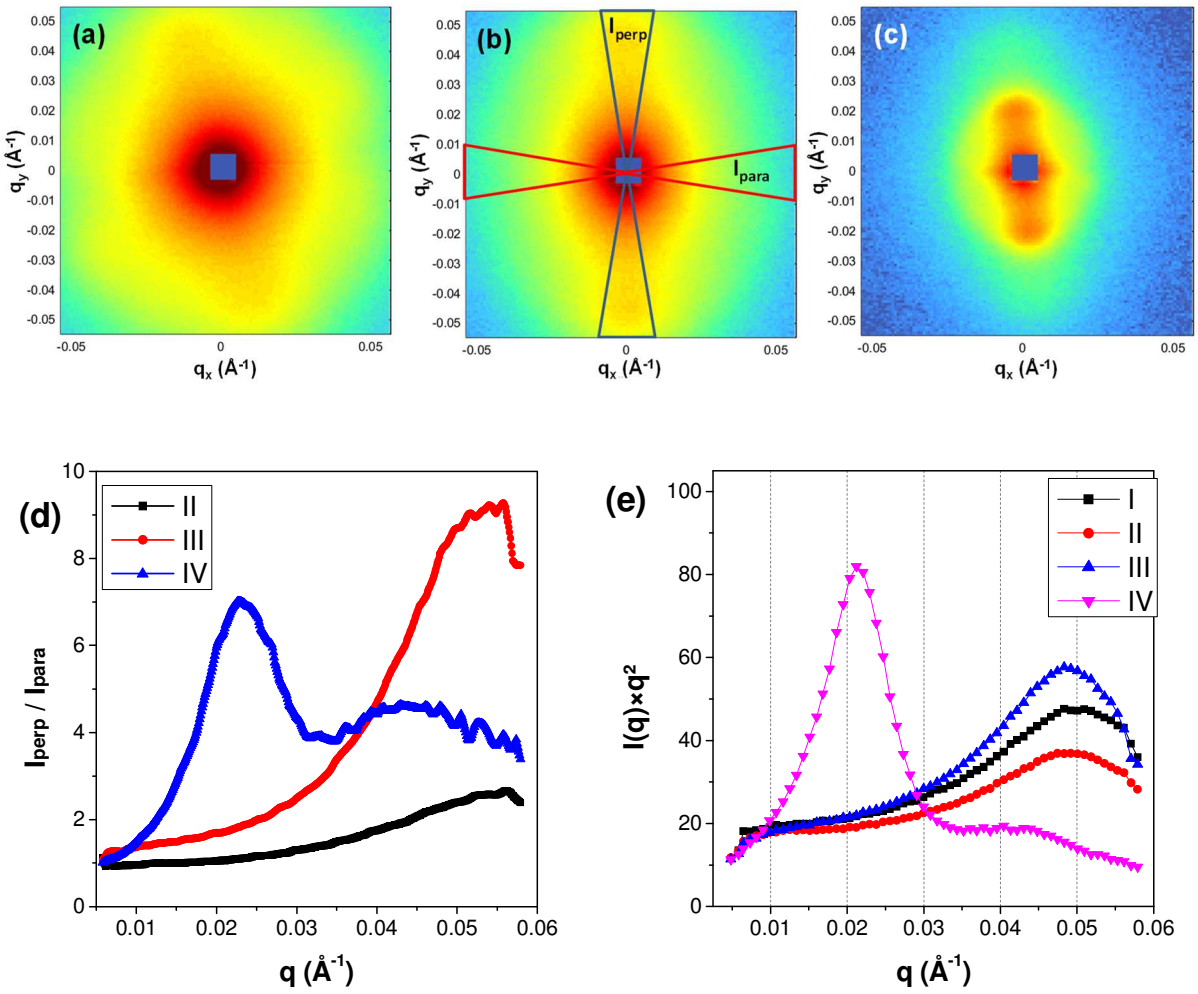

Figure 5. SANS pattern of consolidated magnets: (a) magnet II, NRs d_m = 10.9 nm hot compacted at 450 MPa; (b) magnet III, NRs d_m = 10.9 nm cold compacted at 1 GPa; (c) magnet IV, NRs d_m = 28.3 nm hot compacted at 450 MPa ; (d) Anisotropy ratio I_{perp}/I_{para} for the magnets II, II and IV ; (e) Structure factor $S(q) = I(q)\times q^2$ for the different magnets, with I(q) the intensity scattered perpendicular to the rods.

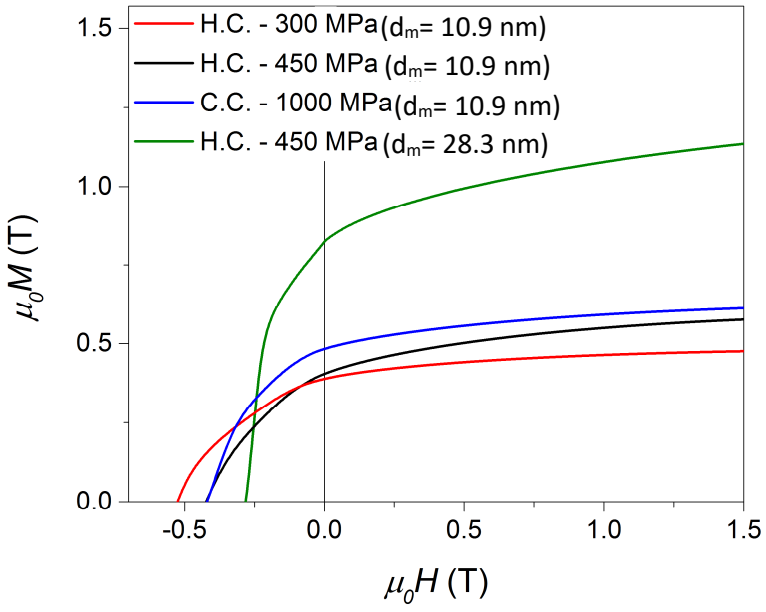

Figure 6. Demagnetization measurements at room temperature of the hot compacted and cold compacted samples. H.C. and C.C. stand for hot compacted and cold compacted, respectively.

References

[1] O. Gutfleisch, M.A. Willard, E. Brück, C.H. Chen, S.G. Sankar, J.P. Liu, Magnetic materials and devices for the 21st century: stronger, lighter, and more energy efficient, Adv. Mater. 23 (7) (2011) 821-842.

[2] N. Jones, The Pull of Stronger Magnets. Nature 472 (2011) 22-23.

[3] J.M.D. Coey, *Magnetism and Magnetic Materials* (Cambridge University Press, Cambridge, **2010**).

[4] J.M. D. Coey, Permanent magnets: Plugging the gap, *Scr. Mater.* 67 (6) (2012) 524-529.

[5] S. Ener, J. Kroder, K. P. Skokov, O. Gutfleisch, The search for room temperature tetragonal phases of Fe-Mn-Ga: A reactive crucible melting approach, J. Alloys Compd. 683 (2016) 198-204 .

[6] D. Goll, R. Loeffler, J. Herbst, R. Karimi, G. Schneider, High-throughput search for new permanent magnet materials, J. Phys. Condens. Matter 26 (6) (2014) 064208.

[7] J. M. D. Coey, New permanent magnets; manganese compounds, J. Phys.: Condens. Matter, 26 (6) (2014) 064211.

[8] S. Muralidhar, J. Gräfe Y.-C. Chen, M. Etter, G. Gregori, S. Ener, S. Sawatzki, K. Hono, O. Gutfleisch, H. Kronmüller, G. Schütz,, E.J. Goering, emperature-dependent first-order reversal curve measurements on unusually hard magnetic low-temperature phase of MnBi, Phys. Rev. B 95(2) (2017) 024413.

[9] S. Ener, K.P. Skokov, D.Y. Karpenkov, M.D. Kuz'min, O. Gutfleisch, Magnet properties of $Mn_{70}Ga_{30}$ prepared by cold rolling and magnetic field annealing, J. Magn. Magn. Mater. 382 (2015) 265-270.

[10] B. Balasubramanian, B. Das , R. Skomski , W. Y. Zhang , D. J. Sellmyer, Novel Nanostructured Rare-Earth-Free Magnetic Materials with High Energy Products, Adv. Mater. 25(42) (2013) 6090-6093.

[11] V.G. Harris, Y. Chen, A. Yang, S. Yoon, Z. Chen, A.L. Geiler, J. Gao, C. N. Chinnasamy, L. H. Lewis, C. Vittoria, E. E. Carpenter, K. J. Carroll, R. Goswami, M A Willard, L. Kurihara, M Gjoka, O. Kalogirou, High coercivity cobalt carbide nanoparticles processed via polyol reaction: a new permanent magnet material, J. Phys. D: Appl. Phys. 43 (16) (2010) 165003.

[12] S. Fujieda, A. Yomogida, K. Shinoda, S. Suzuki, Magnetic Properties of Cobalt-Based Carbide Particles Synthesized by the Polyol Process, IEEE Magnetics Letters, 7 (2016) 1-4.

[13] R. Skomski, J. M. D. Coey, Magnetic anisotropy- How much is enough for a permanent magnet? *Scr. Mater.* 112 (2016) 3–8.

[14] D. J. Sellmyer, Strong Magnets by Self-Assembly, Nature 420 (2002) 374–375.

[15] E. Lottini, A. López-Ortega, G. Bertoni, S. Turner, M. Meledina, G. Van Tendeloo, C. de Julián Fernández, C. Sangregorio, Strongly exchange coupled core| shell nanoparticles with high magnetic anisotropy: a strategy toward rare-earth-free permanent magnets, Chem. Mater. 28 (12) (2016), 4214-4222.

[16] T. Maurer, F. Ott, G. Chaboussant, Y. Soumare, J.-Y. Piquemal, G. Viau, Magnetic nanowires as permanent magnet materials, Appl. Phys. Lett. 91(17) (2007) 172501.

[17] N. Liakakos, T. Blon, C.Achkar, B. Cormary, R. P. Ran, O. Benamara, G. Chaboussant, F. Ott, B. Warot-Fonrose, E. Snoeck, B. Chaudret, K. Soulantica, M. Respaud, Solution epitaxial growth of cobalt nanowires on crystalline substrates for data storage densities beyond 1 Tbit/in^2, Nano Lett. 14(6) (2014) 3481-3486.

[18] E. Anagnostopoulou, B. Grindi, L.–M. Lacroix, F. Ott, I. Panagiotopoulos, G. Viau, Dense arrays of cobalt nanorods as rare-earth free permanent magnets, Nanoscale 8(7) (2016) 4020-4029.

[19] M. Pousthomis, E. Anagnostopoulou, I. Panagiotopoulos, R. Boubekri, W. Fang, F. Ott, K. Aït Atmane, J.-Y. Piquemal, L.-M. Lacroix, G. Viau, Localized magnetization reversal processes in cobalt nanorods with different aspect ratios, Nano Research 8(7) (2015) 2231-2241.

[20] T. M. Kha, F. Schoenstein, F. Zighem, S. Nowak, B. Leridon, N. Jouini, S. Mercone, Effect of stacking faults on the magnetocrystalline anisotropy of hcp Co-based nanowires, J. Magn. Magn. Mater. 422 (2017) 221-226.

[21] K. Gandha, K. Elkins, N. Poudyal, X. Liu, J. P. Liu, High energy product developed from cobalt nanowires, Sci. Rep. 4 (2014) 5345.

[22] I. S. Camara, C. Achkar, N. Liakakos, A. Pierrot, V. Pierron-Bohnes, Y. Henry, K. Soulantica, M. Respaud, T. Blon, M. Bailleul, Enhanced magnetocrystalline anisotropy in an ultra-dense array of air-exposed crystalline cobalt nanowires, Appl. Phys. Lett. 109(20) (2016) 202406.

[23] H. Song, J. Spencer, A. Jander, J. Nielsen, J. Stasiak, V. Kasperchik, P. Dhagat, Inkjet printing of magnetic materials with aligned anisotropy, J. Appl. Phys. 115(17) (2014) 17E308.

[24] N. M. Dempsey, D. Le Roy, H. Marelli-Mathevon, G. Shaw, A. Dias, R. B. G. Kramer, L. Viet Cuong, M. Kustov, L. F. Zanini, C. Villard, K. Hasselbach, C. Tomba, F. Dumas-Bouchiat, Micro-magnetic imprinting of high field gradient magnetic flux sources, Appl. Phys. Lett. 104(26) (2014) 262401.

[25] M. Kandpal, C. Sharan, V. Palaparthy, N. Tiwary, P. Poddar, V. R. Rao, Spin-coatable, photopatternable magnetic nanocomposite thin films for MEMS device applications, RSC Adv. 5(104) (2015) 85741–85747.

[26] M. Han, Z. Li, X. Sun, H. Zhang, Analysis of an in-plane electromagnetic energy harvester with integrated magnet array, Sensors and Actuators A: Physical 219 (2014) 38-46.

[27] N. V. Myung, D.-Y. Park, B.-Y. Yoo, P. T. Sumodjo, Development of electroplated magnetic materials for MEMS, *J. Magn. Magn. Mater.* 265(2) (2003) 189–198.

[28] C.-B. Rong, V. Nandwana, N. Poudyal, J. P. Liu, T. Saito, Y. Wu, M. J. Kramer, Bulk FePt/Fe_3Pt nanocomposite magnets prepared by spark plasma sintering, J. Appl. Phys. 101(9) (2007) 09K515.

[29] C.-B. Rong, V. Nandwana, N. Poudyal, J. P. Liu, M. E. Kozlov, R. H. Baughman, Y. Ding, Z. L. Wang, Bulk FePt-based nanocomposite magnets with enhanced exchange coupling, J. Appl. Phys. 102(2) (2007) 23908.

[30] C. Rong, Y. Zhang, N. Poudyal, D. Wang, M. J. Kramer, J. P. Liu, Bulk $SmCo_5$/α-Fe nanocomposite permanent magnets fabricated by mould-free Joule-heating compaction, J. Appl. Phys. 109(7) (2011) 07A735.

[31] K. Ait Atmane, F. Zighem, Y. Soumare, M. Ibrahim, R.Boubekri, T. Maurer, J. Margueritat, J. –Y. Piquemal, F. Ott, G. Chaboussant, F. Schoenstein, N. Jouini, G. Viau, High temperature structural and magnetic properties of cobalt nanorods, J. Solid State Chem. 197 (2013) 297–303.

[32] N. Ouar, M. A. Bousnina, F. Schoenstein, S. Mercone, O. Brinza, S. Farhat, N. Jouini, Spark Plasma Sintering of $Co_{80}Ni_{20}$ nanopowders synthesized by polyol process and their magnetic and mechanical properties, J. Alloys Comp. 615 (2014) S269–S275.

[33] N. Ouar, F. Schoenstein, S. Mercone, S. Farhat, B Villeroy, B. Leridon, N Jouini, Spark-plasma-sintering magnetic field assisted compaction of $Co_{80}Ni_{20}$ nanowires for anisotropic ferromagnetic bulk materials, J. Appl. Phys. 114(16) (2013) 163907.

[34] http://www-llb.cea.fr/spectros/pdf/paxy-llb.pdf

[35] G. Viau, C. Garcia, T. Maurer, G. Chaboussant, F. Ott, Y. Soumare, J.-Y. Piquemal, Highly crystalline cobalt nanowires with high coercivity prepared by soft chemistry, Phys. Status Solidi A 206(4) (2009) 663-666.

[36] F. Ott, T. Maurer, G. Chaboussant, Y. Soumare, J.-Y. Piquemal, G. Viau, Effects of the shape of elongated magnetic particles on the coercive field, J. Appl. Phys. 105(1) (2009) 013915.

[37] I. Panagiotopoulos, W. Fang, F. Ott, F. Boué, K. Aït-Atmane, J.-Y. Piquemal, G. Viau, Packing fraction dependence of the coercivity and the energy product in nanowire based permanent magnets, J. Appl. Phys. 114(14) (2013) 143902.

[38] P. Toson, A. Asali, W. Wallisch, G. Zickler and J. Fidler, Nanostructured hard magnets: a micromagnetic study, IEEE Trans. Magn. 51(1) (2015) 1-4.

[39] K. Aït Atmane, C. Michel, J.-Y. Piquemal, P. Sautet, P. Beaunier, M. Giraud, M. Sicard, S. Nowak, R. Losno, G. Viau, Control of anisotropic growth of cobalt nanorods in liquid phase: from experiment to theory ... and back, Nanoscale, 6, (2014) 2682 – 2692.

[40] A. Palasyuk, E. Blomberg, R. Prozorov, L. Yue, M. J. Kramer, R. W. Mc Callum, I. E. Anderson, S. Constandines, Advances in characterization of non-rare-earth permanent magnets: Exploring commercial Alnico grades 5–7 and 9, JOM 65(7) (2013) 862-869.

[41] T. Maurer, F. Zighem, F. Ott, G. Chaboussant, G. André, Y. Soumare, J.- Y. Piquemal, G. Viau, C. Gatel, Exchange bias in Co/CoO core-shell nanowires: Role of antiferromagnetic superparamagnetic fluctuations, Phys. Rev. B 80(6) (2009) 064427.

[42] K. Soulantica, F. Wetz, J. Maynadié, A. Falqui, R. P. Tan, T. Blon, B. Chaudret, M. Respaud, Magnetism of single-crystalline Co nanorods, Appl. Phys. Lett. 95 (2009) 152504.

[43] K. Gandha, J. Mohapatra, J. Ping Liu, Coherent magnetization reversal and high magnetic coercivity in Co nanowire assemblies, J. Magn. Magn. Mater. 438 (2017) 41–45.

Supplementary Material

Consolidation of cobalt nanorods: a new route for rare-earth free nanostructured permanent magnets

Semih Ener [a], Evangelia Anagnostopoulou [b], Imants Dirba [a], Lise-Marie Lacroix [b], Frédéric Ott [c], Thomas Blon [b], Jean-Yves Piquemal [d], Konstantin P. Skokov [a], Oliver Gutfleisch [a], Guillaume Viau [b]

[a] *Funktionale Materialien, Institut für Materialwissenschaft, TU Darmstadt, 64287 Darmstadt, Germany*

[b] *Université de Toulouse, Laboratoire de Physique et Chimie des Nano-Objets, UMR 5215 INSA, CNRS, UPS, 135 avenue de Rangueil, F-31077 Toulouse cedex 4, France*

[c] *Laboratoire Léon Brillouin CEA/CNRS, Université Paris-Saclay, CEA Saclay, 91191 Gif sur Yvette, France*

[d] *Université Paris Diderot, Sorbonne Paris Cité, ITODYS, CNRS UMR 7086, 15 rue J.-A. de Baïf, 75205 Paris Cedex 13, France*

X-ray diffraction

Powder X-ray diffraction patterns of cobalt rods with different mean diameter are plotted in Figure S1. These patterns show that the cobalt rods crystallize with the *hcp* structure. No trace of *fcc* phase was detected.

The broadening of the XRD lines is strongly dependent on the (*hkil*) indexes, indicating a strong anisotropy of the crystallites. The (0002) line is always narrower than the $(10\bar{1}0)$ line revealing a longer crystallographic coherence along the *c* axis in agreement with a rod growth axis parallel to the crystallographic *c* axis.

The crystallite size $L_{(10\bar{1}0)}$ measured from the $(10\bar{1}0)$ reflexion broadening using the Scherrer equation was found very close to the particle mean diameter measured by TEM (Fig. S1).

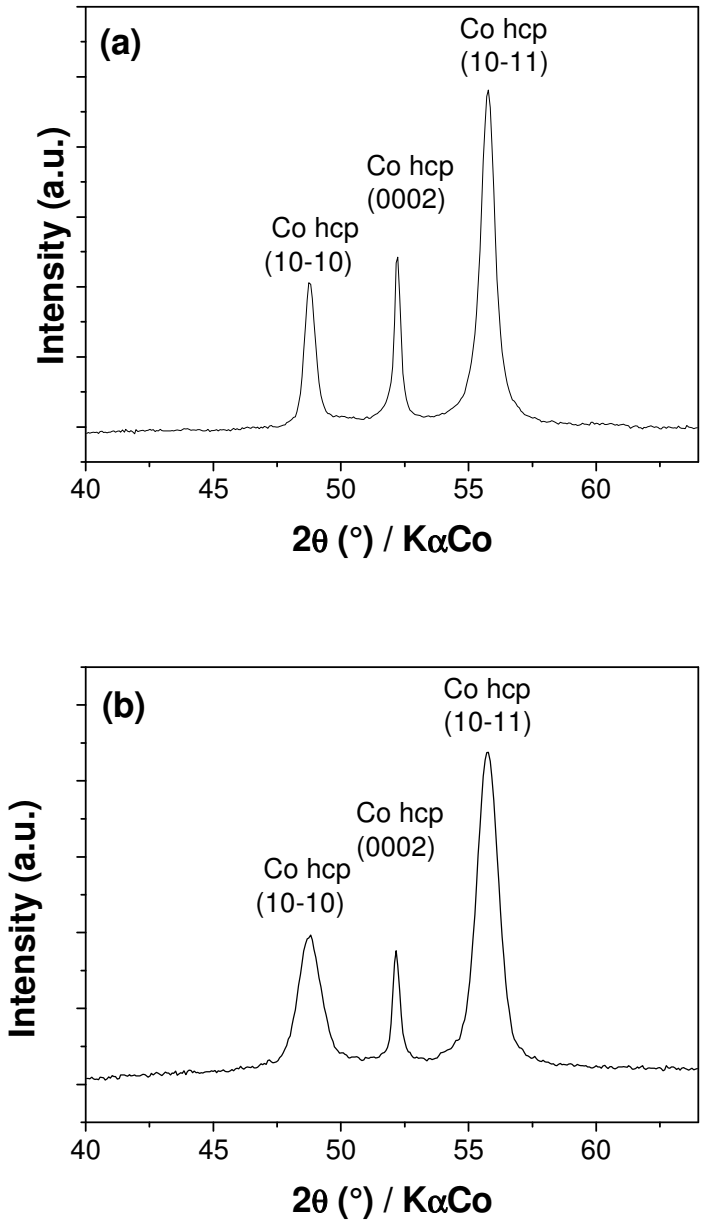

Figure S1. Powder X-ray diffraction patterns of cobalt nanorods randomly oriented (a) mean diameter (TEM) d_m = 28.3 nm and mean crystallite size (XRD) $L_{(10\bar{1}0)}$ = 26 nm ; (b) mean diameter (TEM) d_m = 10.9 nm and mean crystallite size (XRD) $L_{(10\bar{1}0)}$ = 10 nm.

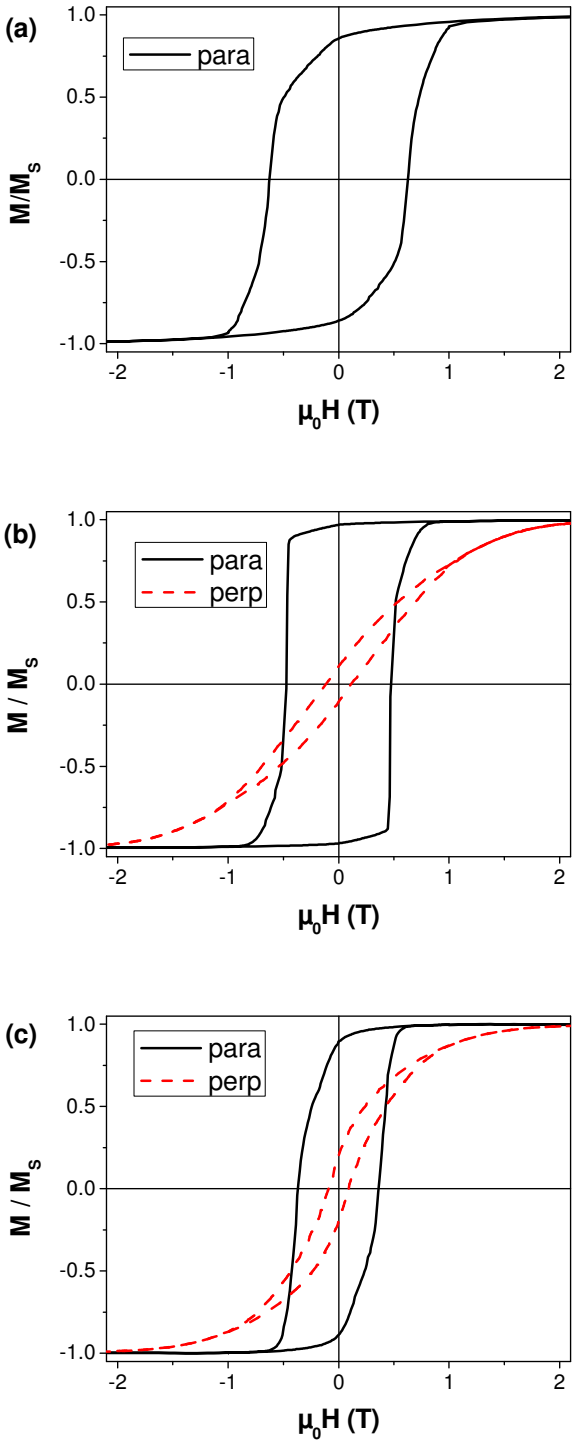

Figure S2. *M(H)* loop of on needle shaped Co NRs assemblies measured with the applied field parallel or perpendicular to the rod alignment direction (a) d_m = 10.9 nm (AR = 18.5) ; (b) d_m = 20.4 nm (AR = 4.5) ; (c) d_m = 28.3 nm (AR = 6.7).

The XRD patterns of the consolidated materials were recorded in the Bragg-Brentano configuration with the rod alignment direction parallel to the diffraction plane. The patterns exhibit the (*hkil*) reflections of the Co *hcp* (Fig. S3). The absence of the Co *fcc* reflections is in agreement with consolidation temperature below the *hcp* → *fcc* phase transition. Broad peaks corresponding to the CoO reflections are also present on the XRD patterns showing a slight oxidation of the rods (Fig. S3).

The comparison with the powder XRD patterns shows an enhancement of the intensity of the reflections $(10\bar{1}0)$ and $(11\bar{2}0)$ in the pattern of the consolidated magnets while the (0002) is nearly extinguished. These two features are in good agreement with a preferential in-plane orientation of the nanorods in the consolidated magnets (Fig. S4).

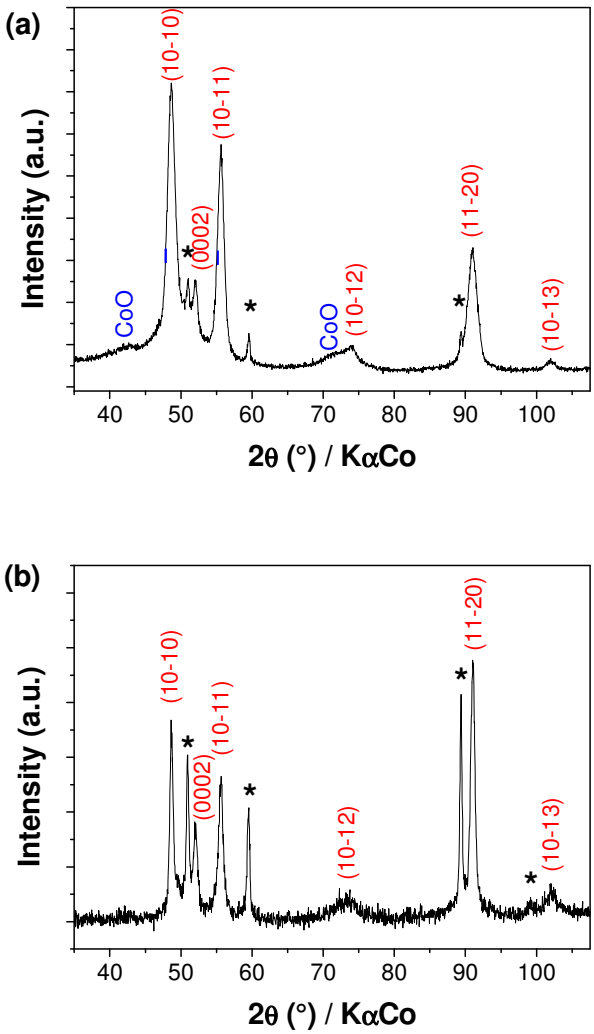

Figure S3. X-ray diffraction pattern of consolidated cobalt nanorods measured in θ-θ configuration: (a) Co NRs with a mean diameter of 10.9 nm consolidated under 1 GPa at room temperature (magnet III); (b) Co NRs with a mean diameter of 28.3 nm consolidated under 450 MPa at 180°C (magnet IV). Peaks marked with a (*) correspond to the sample holder.

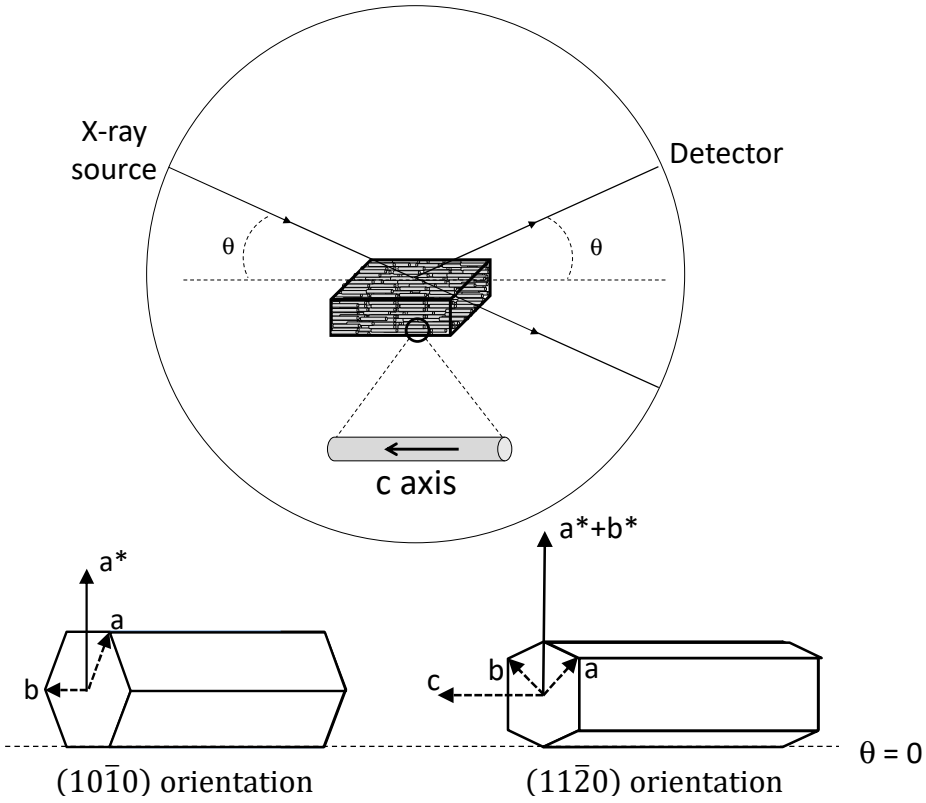

Figure S4. Ideal sketch of a nanorod assembly perfectly oriented in the diffraction plane illustrating the absence of (00*l*) reflections in the XRD pattern recorded in θ-θ configuration. At the opposite the intensities of the reflections $(10\bar{1}0)$ and $(11\bar{2}0)$ are expected to be enhanced in comparison with the powder XRD pattern.

Determination of the inter-rod distance using Small Angle Neutron Scattering (SANS)

The SANS intensity $I(q)$ is a combination of structure factor $S(q)$ characterizing the position correlations between the objects and a form factor characterizing the shape of the scattering objects: $I(q) \propto S(q) * P(q)$. The information about the wire position correlation is contained in $S(Q)$. We empirically assume that the form factor follows a q^{-2} dependence as observed from the curve shape outside the correlation peak. Hence the structure factor can be plotted as $S(q) \propto I(q)\ x\ q^2$. Figure S6(a) shows the scattered intensity for the magnet IV alongside a q^{-2} dependence.

The structure factor of the different samples are presented on Figure S6(b) as $S(q) = I(q)\ x\ q^2$. In the case of magnet IV, the obtained $S(q)$ has the expected shape. It starts from zero, presents a large peak corresponding the first neighbor correlation distance and is then rather flat. A hint of the second order correlation peak can even be observed. In the case of the magnets I, II and III, prepared with the 11 nm rods, the correlation peak is shifted toward the high q range in agreement with a shorter inter-rod distance. From the correlation peak positon q_{peak} it is possible to extract the inter-rod distance as $D = 2\pi / q_{peak}$. One can note that for the magnets I, II, III the inter-rod distance is not changed at all whatever the compaction process. The observed changes in the magnetic properties are essentially linked to misalignment due to temperature effects.

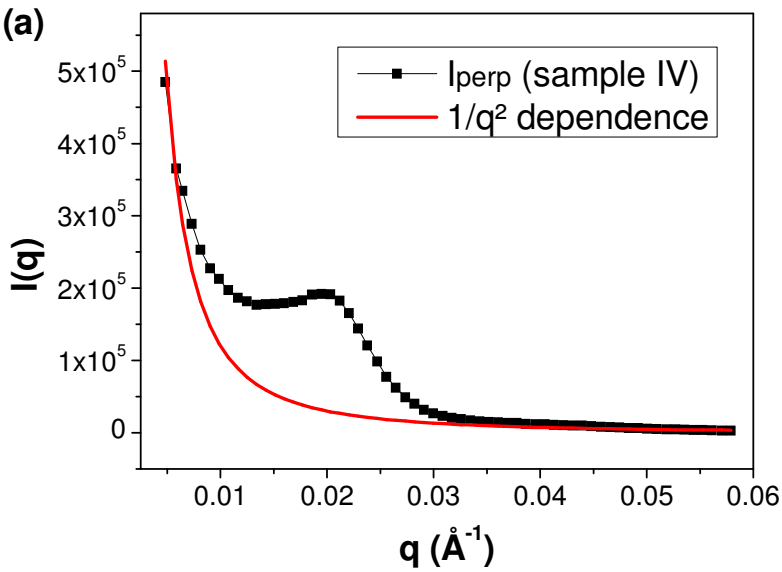

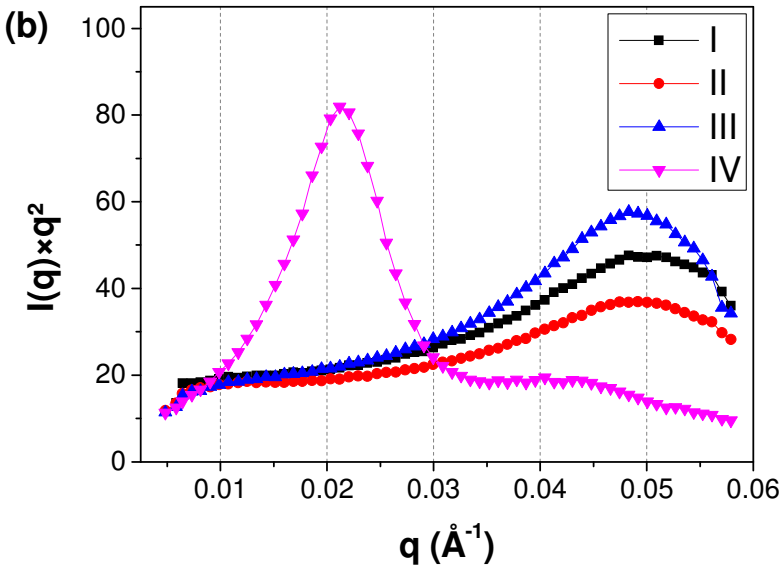

Figure S6.
(a) Scattered intensity I_{perp} for the magnet IV alongside a $1/q^2$ dependence;
(b) Structure factor $S(q) = I(q)\times q^2$ for the different magnets, with I(q) the intensity scattered perpendicular to the rods.